

Hybrid Beamforming with Dynamic Subarrays and Low-resolution PSs for mmWave MU-MISO Systems

Hongyu Li, *Student Member, IEEE*, Ming Li, *Senior Member, IEEE*, and Qian
Liu, *Member, IEEE*,

Abstract

Analog/digital hybrid beamforming architectures with large-scale antenna arrays have been widely considered in millimeter wave (mmWave) communication systems because they can address the tradeoff between performance and hardware efficiency compared with traditional fully-digital beamforming. Most of the prior work on hybrid beamforming focused on fully-connected architecture or partially-connected scheme with fixed-subarrays, in which the analog beamformers are usually realized by infinite-resolution phase shifters (PSs). In this paper, we introduce a novel hybrid beamforming architecture with *dynamic* subarrays and hardware-efficient *low-resolution* PSs for mmWave multiuser multiple-input single-output (MU-MISO) systems. By dynamically connecting each RF chain to a non-overlap subarray via a switch network and PSs, we can exploit multiple-antenna and multiuser diversities to mitigate the performance loss due to the use of practical low-resolution PSs. An iterative hybrid beamformer design algorithm is first proposed based on fractional programming (FP), aiming at maximizing the sum-rate performance of the MU-MISO system. In an effort to reduce the complexity, we also present a simple heuristic hybrid beamformer design algorithm for the dynamic subarray scheme. Extensive simulation results demonstrate the advantages of the proposed hybrid beamforming architecture with dynamic subarrays and low-resolution PSs compared to existing fixed-subarray schemes.

Index Terms

This paper is supported by the National Natural Science Foundation of China (Grant No. 61671101, 61601080, and 61761136019).

H. Li and M. Li are with the School of Information and Communication Engineering, Dalian University of Technology, Dalian 116024, China, (e-mail: hongyuli@mail.dlut.edu.cn, mli@dlut.edu.cn).

Q. Liu is with the School of Computer Science and Technology, Dalian University of Technology, Dalian 116024, China, (e-mail: qianliu@dlut.edu.cn).

Millimeter wave (mmWave) communications, hybrid beamforming, dynamic subarrays, low-resolution phase shifters (PSs), multiple-input single-output (MISO).

I. INTRODUCTION

Millimeter wave (mmWave) communications have been deemed as one of key enabling technologies in 5G and beyond networks because of the significant advantages of providing multi-gigahertz frequency bandwidth and high data rate [1], [2]. Thanks to small antenna size at mmWave frequencies, a large-scale antenna array can be packed into a small area. This feature facilitates the implementation of massive multiple-input multiple-output (MIMO) in mmWave systems, which can provide sufficient beamforming gains to combat the severe path loss in mmWave channels [3], [4]. Nevertheless, realizing the beamforming with large-scale antenna arrays is not straightforward in mmWave systems. Conventional fully-digital beamforming architecture needs to equip one dedicated radio-frequency (RF) chain (including analog-to-digital/digital-to-analog converter (ADC/DAC), etc.) to each antenna. Unfortunately, this fully-digital beamforming architecture cannot be practically employed in mmWave massive MIMO systems due to the unaffordable cost and power consumption of large numbers of mmWave RF chains and other hardware components [5], [6]. Recently, analog/digital hybrid beamforming has been advocated as a practical solution for mmWave massive MIMO systems to balance the system performance and hardware efficiency [7]. The hybrid beamforming architecture employs only a few expensive RF chains to realize low-dimensional digital beamformers and utilizes a large number of cost-efficient phase shifters (PSs) to implement high-dimensional analog beamformers. While the analog beamformers in the RF domain can provide sufficient beamforming gain to compensate for the huge path loss of mmWave channel, the digital beamformers in the baseband domain are able to offer the flexibility to realize multiuser/multiplexing techniques. Because of its efficiency and effectiveness in mmWave systems, hybrid beamforming has attracted extensive attention from both academia and industry in recent years.

A. *Prior Work*

Two typical hybrid beamforming architectures have been widely considered for mmWave MIMO systems, i.e. fully-connected architecture as shown in Fig. 1(a) and partially-connected architecture as

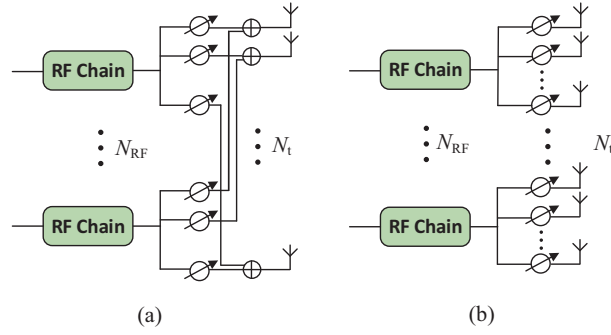


Fig. 1. Traditional hybrid beamforming architectures: (a) fully-connected; (b) partially-connected (fixed-subarray without overlapping).

shown in Fig. 1(b). In the fully-connected hybrid beamforming structure, each RF chain is connected to all antennas via an analog network of PSs. The challenge in designing such hybrid beamformer mainly lays in the practical constraints of PSs, such as constant modulus. In point-to-point mmWave MIMO systems, maximizing spectral efficiency is often approximated by minimizing the Euclidean distance between the hybrid beamformer and the fully-digital beamformer [8]-[10]. Codebook-based hybrid beamformer designs are also widely used [11]-[13], in which the analog beamformers are picked from certain candidate vectors, such as array response vectors and discrete Fourier transform (DFT) beamformers. Hybrid beamformer design for mmWave multiuser systems have also been investigate in [14]-[17]. While fully-connected hybrid beamforming enjoys satisfactory spectral efficiency performance close to that obtained with fully-digital solutions, it still suffers from relatively high power consumption and hardware complexity due to the use of a large number of PSs. Therefore, partially-connected architecture [18]-[21], in which each RF chain is connected to a fixed disjoint subset of antennas, has been proposed to reduce the number of PSs and further decrease the power consumption and hardware complexity.

The aforementioned hybrid beamformer designs generally assume the use of *infinite/high-resolution* PSs, which require complicated hardware circuits and have high energy consumption at mmWave frequencies [6]. Thus, other than reducing the number of PSs, using cost-effective and energy-saving *low-resolution* PSs to implement analog beamformers is another hardware-efficient approach [22]. Several literatures have investigated the hybrid beamformer design with finite/low-resolution PSs for the fully-connected architecture [23]-[26]. In order to achieve the maximum hardware efficiency, [27], [28] investigated partially-connected architectures with 1-bit (i.e. binary) PSs for a point-to-point mmWave MIMO system. However, the performance of traditional partially-connected schemes with fixed-subarray and low-resolution PSs is

not always satisfactory due to the following two reasons: *i)* The employment of low-resolution PSs makes it difficult to finely control the beam and thus will cause notable performance degradation; *ii)* fixed-subarray architecture limits the flexibility of large antenna arrays and further influences beamforming accuracy. Therefore, a meaningful research direction is seeking efficient solutions to tackle above two problems for partially-connected hybrid beamforming architectures with low-resolution PSs.

Recently, dynamic connection/mapping strategy, which adaptively partitions all transmit antennas into several subarrays associated with different RF chains, has been proposed to mitigate the performance degradation caused by fixed-subarrays. Several literatures have demonstrated the benefits on both spectral efficiency and energy efficiency by applying the dynamic connection strategy in the hybrid beamforming with high/finite resolution PSs [29]-[34]. Moreover, recent works [35], [36] illustrate that adaptively selecting a subset of transmit antennas from a large-scale antenna array can exploit the augmented antenna diversity to effectively compensate for the accuracy loss of low-resolution PSs. Motivated by these findings, we attempt to take full advantage of both the flexibility of the dynamic antenna scheme and the multiple-antenna diversity of large-scale antenna arrays to enhance the performance of the partially-connected hybrid beamforming with low-resolution PSs.

B. Contributions

In this paper, we consider the problem of the hybrid beamformer design for mmWave multiuser multiple-input single-output (MU-MISO) systems. The contributions of this paper are summarized as follows:

- We introduce an efficient hybrid beamforming architecture with dynamic subarray and low-resolution PSs. In an effort to mitigate the performance loss due to the use of low-resolution PSs, each RF chain is dynamically connected to a disjoint subset of the total transmit antennas to exploit the multiple-antenna and multiuser diversities.
- With the aid of fractional programming (FP), an effective hybrid beamformer design algorithm is proposed to maximize the sum-rate performance of the mmWave MU-MISO system.
- In order to reduce the time complexity, we also develop a simple heuristic hybrid beamformer design algorithm to alternatively update the analog beamformer and digital beamformer until a convergence solution is obtained.

- The time complexities of the proposed FP-based and heuristic hybrid beamformer designs are analyzed and compared.
- The effectiveness of two proposed hybrid beamformer designs is validated by extensive simulation results, which illustrate that both two algorithms can remarkably outperform traditional fixed-subarray schemes.

C. Notations:

The following notations are used throughout this paper. \mathbf{a} and \mathbf{A} indicate column vectors and matrices, respectively. $(\cdot)^*$ denotes the conjugate operation of a complex number. $(\cdot)^T(\cdot)^H$ and $(\cdot)^{-1}$ denote the transpose, conjugate-transpose operation, and inversion for a matrix, respectively. $\mathbb{E}\{\cdot\}$ represents statistical expectation. $\Re\{\cdot\}$ extracts the real part of a complex number. \mathbf{I}_L indicates an $L \times L$ identity matrix. \mathbb{C} denotes the set of complex numbers. $|\mathcal{A}|$ denotes the cardinality of set \mathcal{A} . $\|\mathbf{A}\|_F$ denotes the Frobenius norm of matrix \mathbf{A} . $\|\mathbf{a}\|_0$ is the 0-norm of vector \mathbf{a} . Finally, $\mathbf{A}(i, :)$ and $\mathbf{A}(i, j)$ denote the i -th row and (i, j) -th element of matrix \mathbf{A} , respectively.

II. SYSTEM MODEL AND PROBLEM FORMULATION

A. System Model

We consider a mmWave downlink MU-MISO system as illustrated in Fig. 2. The base station (BS) employs a uniform plane array (UPA) with N_x antennas in horizontal direction and N_y antennas in vertical direction. The total number of antennas is $N_t = N_x \times N_y$ and the number of RF chains is N_{RF} , $N_{\text{RF}} \ll N_t$. By the hybrid beamforming technology, the BS can simultaneously communicate with K single-antenna users. In this paper, we assume the number of RF chains at the BS is greater than or equal to the number of users, i.e. $N_{\text{RF}} \geq K$. The information symbols of K users are firstly precoded by a digital beamforming matrix $\mathbf{F}_{\text{BB}} \triangleq [\mathbf{f}_{\text{BB},1}, \dots, \mathbf{f}_{\text{BB},K}] \in \mathbb{C}^{N_{\text{RF}} \times K}$. After being up-converted to the RF domain via N_{RF} RF chains, the signals are further precoded in the RF domain by N_t low-resolution PSs. Particularly, each RF chain will be dynamically connected to a disjoint set of antennas via a switch (SW) network and corresponding PSs. Several previous works [37]-[39] have demonstrated the feasibility and effectiveness of employing switches in hybrid beamforming architectures for mmWave MIMO systems. By mapping

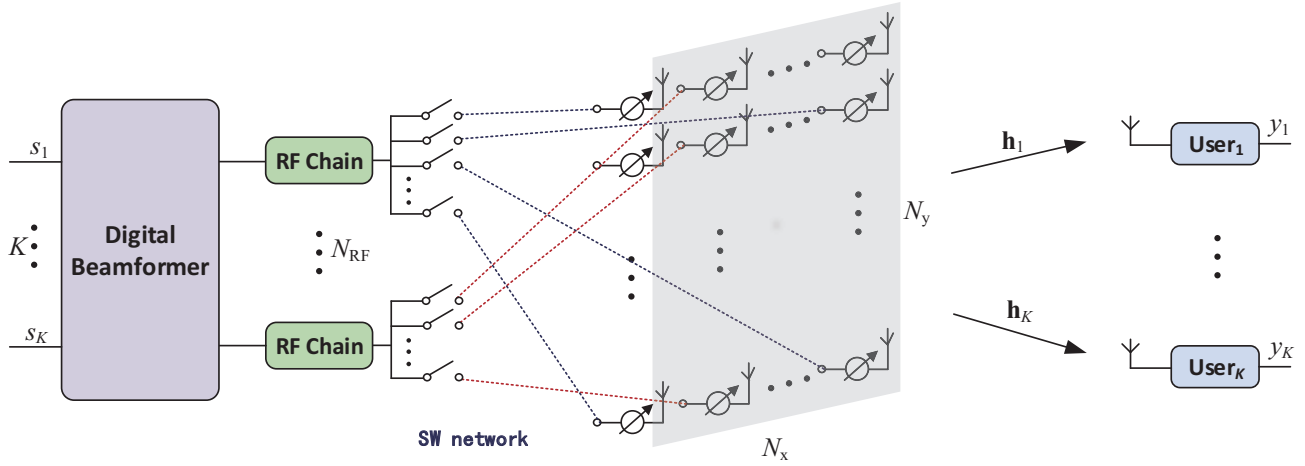


Fig. 2. Hybrid beamforming with dynamic subarrays and low-resolution PSs for mmWave MU-MISO system.

each digitally-precoded data stream to one dynamic antenna subarray, the analog precoding is carried out using a set of corresponding low-resolution PSs, each of which has a constant magnitude $\frac{1}{\sqrt{N_t}}$ and quantized phases controlled by the number of bits B . The possible phases of each PS are within a set $\mathcal{F} \triangleq \{\frac{1}{\sqrt{N_t}}e^{j\frac{2\pi b}{2^B}} | b = 0, 1, \dots, 2^B - 1\}$. Obviously, the beamforming gains for each user can be easily adjusted by changing the sizes of subarrays. More importantly, by dynamically selecting antennas and tuning the phases of the associated PSs, the multi-antenna and multiuser diversities can be utilized to appropriately compensate the accuracy loss due to the use of low-resolution PSs. Therefore, the signal of each RF chain can dynamically select the optimal antenna subarray and employ the optimal corresponding analog beamformer according to the instantaneous channel state information (CSI) of all users, in such a way to enhance the downlink multiuser transmission performance.

To facilitate the dynamic subarray analog beamformer design, we define the analog beamformer matrix as $\mathbf{F}_{\text{RF}} \in \{\mathcal{F}, 0\}^{N_t \times N_{\text{RF}}}$. Specifically, if the k -th RF chain is connected to the i -th antenna via a low-resolution PS, then the corresponding element of analog beamformer $\mathbf{F}_{\text{RF}}(i, k) \in \mathcal{F}$ has a nonzero phase value; otherwise, $\mathbf{F}_{\text{RF}}(i, k) = 0$. To guarantee no overlap among different subarrays, the analog beamformer has only one nonzero element in each row, i.e. $\|\mathbf{F}_{\text{RF}}(i, :)\|_0 = 1, i = 1, \dots, N_t$.

Then, the transmitted signal at the BS can be expressed as

$$\mathbf{x} = \sum_{k=1}^K \mathbf{F}_{\text{RF}} \mathbf{f}_{\text{BB},k} s_k, \quad (1)$$

where $s_k \in \mathbb{C}, k = 1, \dots, K$, is the transmit symbol for the k -th user. All the information symbols are

independent within a user stream and across the users, $\mathbb{E}\{|s_k|^2\} = 1$.

Consider a narrow-band system, the received signal of the k -th user can be modeled as

$$y_k = \mathbf{h}_k^H \sum_{k=1}^K \mathbf{F}_{\text{RF}} \mathbf{f}_{\text{BB},k} s_k + n_k, \quad (2)$$

where $\mathbf{h}_k \in \mathbb{C}^{N_t}$, $k = 1, \dots, K$, denotes the channel vector between the BS and the k -th user and $n_k \sim \mathcal{CN}(0, \sigma_k^2)$, $k = 1, \dots, K$, is the independent and identically distributed (i.i.d.) complex Gaussian noise with variance σ_k^2 .

B. Channel Model

As many literatures claimed [3]-[5], [11], [40], mmWave channel is expected to have limited scattering due to the highly directional propagation characteristic at the mmWave frequencies. Therefore, the mmWave channel can be simply modeled as a sum of multiple propagation paths. Under this classic model, the k -th channel vector can be formulated as

$$\mathbf{h}_k = \sqrt{\frac{N_t}{L_k}} \sum_{l=1}^{L_k} \alpha_{k,l} \mathbf{a}(\phi_{k,l}, \theta_{k,l}), \quad (3)$$

where $\sqrt{\frac{N_t}{L_k}}$ is a normalization factor, L_k is the number of paths and $\alpha_{k,l} \sim \mathcal{CN}(0, 1)$ is the complex gain of the l -th path for the k -th user. $\mathbf{a}(\phi_{k,l}, \theta_{k,l})$ denotes the transmit steering vector for the k -th user of the l -th path with horizontal and vertical angles of departure (AoD) of $\phi_{k,l}$ and $\theta_{k,l}$, respectively. For an $N_x \times N_y$ UPA with N_t total transmit antennas and inter-antenna space d , the transmit steering vector of the l -th path for the k -th user is given by [19]

$$\mathbf{a}(\phi_{k,l}, \theta_{k,l}) = \mathbf{a}_x(\phi_{k,l}, \theta_{k,l}) \otimes \mathbf{a}_y(\theta_{k,l}), \quad (4)$$

where \otimes is the Kronecker-product operation, $\mathbf{a}_y(\theta_{k,l})$ denotes the vertical steering vector of the l -th path for the k -th user, which has a form of

$$\mathbf{a}_y(\theta_{k,l}) = \frac{1}{\sqrt{N_y}} [1, e^{j\frac{2\pi}{\lambda} d \cos \theta_{k,l}}, \dots, e^{j(N_y-1)\frac{2\pi}{\lambda} d \cos \theta_{k,l}}]^T, \quad (5)$$

where λ denotes the wavelength of the signal. $\mathbf{a}_x(\phi_{k,l}, \theta_{k,l})$ denotes the horizontal steering vector of the l -th path for the k -th user, which is given by

$$\mathbf{a}_x(\phi_{k,l}, \theta_{k,l}) = \frac{1}{\sqrt{N_x}} [1, e^{j\frac{2\pi}{\lambda} d \sin \theta_{k,l} \sin \phi_{k,l}}, \dots, e^{j(N_x-1)\frac{2\pi}{\lambda} d \sin \theta_{k,l} \sin \phi_{k,l}}]^T. \quad (6)$$

In this paper, we assume the knowledge of \mathbf{h}_k for each user is known perfectly and instantaneously to the BS, which can be obtained by the channel estimation with uplink training [4], [39].

C. Problem Formulation

The sum-rate of the MU-MISO downlink system is given by

$$R = \sum_{k=1}^K \log_2(1 + \text{SINR}_k), \quad (7)$$

where SINR_k is the signal-to-interference-plus-noise ratio (SINR) of the k -th user, which can be written as

$$\text{SINR}_k = \frac{|\mathbf{h}_k^H \mathbf{F}_{\text{RF}} \mathbf{f}_{\text{BB},k}|^2}{\sum_{j \neq k} |\mathbf{h}_k^H \mathbf{F}_{\text{RF}} \mathbf{f}_{\text{BB},j}|^2 + \sigma_k^2}, \quad \forall k. \quad (8)$$

The objective of this paper is to jointly design the digital beamformer \mathbf{F}_{BB} and analog beamformer \mathbf{F}_{RF} to maximize the sum-rate of the MU-MISO downlink system, subject to the following constraints: *i*) constant amplitude and discrete phases of PSs, i.e. $\mathbf{F}_{\text{RF}}(i, j) \in \{0, \mathcal{F}\}, i = 1, \dots, N_t, j = 1, \dots, N_{\text{RF}}$; *ii*) non-overlapping dynamic mapping, i.e. $\|\mathbf{F}_{\text{RF}}(i, :)\|_0 = 1, i = 1, \dots, N_t$; *iii*) transmit power constraint, i.e. $\|\mathbf{F}_{\text{RF}} \mathbf{F}_{\text{BB}}\|_F^2 = P$, where P is the transmit power. With above constraints, the problem can be formulated as

$$\begin{aligned} \{\mathbf{F}_{\text{RF}}^*, \mathbf{F}_{\text{BB}}^*\} &= \arg \max R \\ \text{s.t. } \mathbf{F}_{\text{RF}}(i, j) &\in \{0, \mathcal{F}\}, \forall i, j, \\ \|\mathbf{F}_{\text{RF}}(i, :)\|_0 &= 1, \forall i, \\ \|\mathbf{F}_{\text{RF}} \mathbf{F}_{\text{BB}}\|_F^2 &= P. \end{aligned} \quad (9)$$

Obviously, the optimization problem (9) is non-convex and difficult to solve due to the discrete phases of low-resolution PSs and the l_0 norm constraint. To tackle the difficulties in (9), we first propose an iterative design algorithm with satisfactory performance based on the theory of FP, then we develop a simple heuristic method to further reduce the time complexity.

III. FP-BASED HYBRID BEAMFORMER DESIGN

We start by analyzing the characteristic of the objective in (7). The objective is computed as $\sum_{k=1}^K \log(1 + \text{SINR}_k)$, which is a typical function of multiple fractional parameters (i.e. SINRs). Motivated by the findings in [41], [42] which can use FP to solve this multiple-ratio problem (such as fully-digital beamforming

and power allocation problem in multiuser MIMO systems), we attempt to equivalently transform the original problem to a solvable form. Then, with the newly transformed objective function, we propose to iteratively design the analog beamformer and digital beamformer.

A. Transformation of objective function

We begin with taking the ratio parts $\text{SINR}_k, k = 1, \dots, K$, out of the logarithm. Based on the *Lagrangian Dual Transform* [42], we present the following proposition.

Proposition 1. The objective function in (9) is equivalent to

$$f_r(\mathbf{F}_{\text{RF}}, \mathbf{F}_{\text{BB}}, \mathbf{r}) = \sum_{k=1}^K \log_2(1 + r_k) - \sum_{k=1}^K r_k + \sum_{k=1}^K \underbrace{\frac{(1 + r_k) |\mathbf{h}_k^H \mathbf{F}_{\text{RF}} \mathbf{f}_{\text{BB},k}|^2}{\sum_{j=1}^K |\mathbf{h}_k^H \mathbf{F}_{\text{RF}} \mathbf{f}_{\text{BB},j}|^2 + \sigma_k^2}}_{\text{fractional term}}, \quad (10)$$

when each element of the auxiliary variable vector $\mathbf{r} \triangleq [r_1, \dots, r_K]^T$ has the following optimal value:

$$r_k^* = \frac{|\mathbf{h}_k^H \mathbf{F}_{\text{RF}} \mathbf{f}_{\text{BB},k}|^2}{\sum_{j \neq k} |\mathbf{h}_k^H \mathbf{F}_{\text{RF}} \mathbf{f}_{\text{BB},j}|^2 + \sigma_k^2}, \forall k. \quad (11)$$

Proof: See Appendix A. ■

By Proposition 1, with the same constraints, the problems of (9) and maximizing (10) are equivalent in the sense that $\{\mathbf{F}_{\text{RF}}, \mathbf{F}_{\text{BB}}\}$ are solutions to (9) if and only if they are also solutions to maximize (10), i.e. $\{\mathbf{F}_{\text{RF}}^*, \mathbf{F}_{\text{BB}}^*\}$ are common optimal solutions of these two problems. Therefore, the original objective in (7) can be firstly transformed into an equivalent function $f_r(\mathbf{F}_{\text{RF}}, \mathbf{F}_{\text{BB}}, \mathbf{r})$ as shown in (10). Unfortunately, the hybrid beamformer design problem is still intractable due to the complicated form of the sum of K fractional term (the last term as inclosed in (10)). Next, in an effort to facilitate the analog beamformer and digital beamformer design for fixed $r_k^*, k = 1, \dots, K$, we attempt to apply *Quadratic Transform* [42] on the fractional term. To achieve this goal, we develop the following proposition.

Proposition 2. The fractional term in objective function (10)

$$\frac{(1 + r_k) |\mathbf{h}_k^H \mathbf{F}_{\text{RF}} \mathbf{f}_{\text{BB},k}|^2}{\sum_{j=1}^K |\mathbf{h}_k^H \mathbf{F}_{\text{RF}} \mathbf{f}_{\text{BB},j}|^2 + \sigma_k^2}, \forall k, \quad (12)$$

is equivalent to

$$2\sqrt{1 + r_k} \Re\{t_k^* \mathbf{h}_k^H \mathbf{F}_{\text{RF}} \mathbf{f}_{\text{BB},k}\} - |t_k|^2 \mathbf{C}_k, \forall k, \quad (13)$$

when the auxiliary variables $t_k, k = 1, \dots, K$, have the following optimal values:

$$t_k^* = \frac{\sqrt{1 + r_k} \mathbf{h}_k^H \mathbf{F}_{\text{RF}} \mathbf{f}_{\text{BB},k}}{\mathbf{C}_k}, \forall k, \quad (14)$$

where

$$\mathbf{C}_k \triangleq \sum_{j=1}^K |\mathbf{h}_k^H \mathbf{F}_{\text{RF}} \mathbf{f}_{\text{BB},j}|^2 + \sigma_k^2, \forall k. \quad (15)$$

Proof: See Appendix B. ■

By Proposition 2, function (10) can be further reformulated as

$$f_q(\mathbf{F}_{\text{RF}}, \mathbf{F}_{\text{BB}}, \mathbf{r}, \mathbf{t}) = \sum_{k=1}^K \log_2(1 + r_k) - \sum_{k=1}^K r_k + \sum_{k=1}^K (2\sqrt{1 + r_k} \Re\{t_k^* \mathbf{h}_k^H \mathbf{F}_{\text{RF}} \mathbf{f}_{\text{BB},k}\} - |t_k|^2 \mathbf{C}_k), \quad (16)$$

where $\mathbf{t} \triangleq [t_1, \dots, t_K]^T$. Now, with auxiliary variable vectors \mathbf{r} and \mathbf{t} , the optimization problem (9) can be transformed as

$$\begin{aligned} \{\mathbf{F}_{\text{RF}}^*, \mathbf{F}_{\text{BB}}^*, \mathbf{r}^*, \mathbf{t}^*\} &= \arg \max f_q(\mathbf{F}_{\text{RF}}, \mathbf{F}_{\text{BB}}, \mathbf{r}, \mathbf{t}) \\ \text{s.t. } \mathbf{F}_{\text{RF}}(i, j) &\in \{0, \mathcal{F}\}, \forall i, j, \\ \|\mathbf{F}_{\text{RF}}(i, :)\|_0 &= 1, \forall i, \\ \|\mathbf{F}_{\text{RF}} \mathbf{F}_{\text{BB}}\|_F^2 &= P. \end{aligned} \quad (17)$$

To efficiently solve this problem, we propose to iteratively update the variables $\mathbf{F}_{\text{RF}}, \mathbf{F}_{\text{BB}}, \mathbf{r}$, and \mathbf{t} to find at each iteration the conditionally optimal solution of one variable matrix/vector given others. While the conditionally optimal \mathbf{r} and \mathbf{t} are already shown in (11) and (14), respectively, in the following, we turn to develop the iterative design of the digital beamformer and analog beamformer with given optimal \mathbf{r}^* and \mathbf{t}^* .

To facilitate the analog and digital beamformer design, we rewrite the objective function in (17) as the following form:

$$f_q(\mathbf{F}_{\text{RF}}, \mathbf{F}_{\text{BB}}, \mathbf{r}, \mathbf{t}) = \sum_{k=1}^K \log_2(1 + r_k) - \sum_{k=1}^K r_k - \sum_{k=1}^K |t_k|^2 \sigma_k^2 + \delta, \quad (18)$$

where

$$\delta \triangleq \sum_{k=1}^K 2\sqrt{1 + r_k} \Re\{t_k^* \mathbf{h}_k^H \mathbf{F}_{\text{RF}} \mathbf{f}_{\text{BB},k}\} - \sum_{k=1}^K \sum_{j=1}^K |t_j|^2 |\mathbf{h}_j^H \mathbf{F}_{\text{RF}} \mathbf{f}_{\text{BB},k}|^2, \quad (19)$$

$$= \sum_{k=1}^K (\sqrt{1 + r_k} (t_k^* \mathbf{h}_k^H \mathbf{F}_{\text{RF}} \mathbf{f}_{\text{BB},k} + \mathbf{f}_{\text{BB},k}^H \mathbf{F}_{\text{RF}}^H \mathbf{h}_k t_k) - \mathbf{f}_{\text{BB},k}^H \mathbf{A} \mathbf{f}_{\text{BB},k}), \quad (20)$$

with

$$\mathbf{A} \triangleq \mathbf{F}_{\text{RF}}^H \sum_{j=1}^K |t_j|^2 \mathbf{h}_j \mathbf{h}_j^H \mathbf{F}_{\text{RF}}. \quad (21)$$

From the above equivalent transformation we can see, when \mathbf{r} and \mathbf{t} are all fixed, maximizing f_q in (17) is equivalent to maximizing the last term of f_q in (18), i.e. δ which is given by (20). Roughly speaking, δ can be deemed as a summation of transformed SINRs of K users, where the ratio form of each SINR is converted to the difference between useful power and multiuser interference. Motivated by this finding, the conditionally optimal analog beamformer and digital beamformer can be determined by the following problem:

$$\begin{aligned} \{\mathbf{F}_{\text{RF}}^*, \mathbf{F}_{\text{BB}}^*\} &= \arg \max \delta \\ \text{s.t. } \mathbf{F}_{\text{RF}}(i, j) &\in \{0, \mathcal{F}\}, \forall i, j, \\ \|\mathbf{F}_{\text{RF}}(i, :)\|_0 &= 1, \forall i, \\ \|\mathbf{F}_{\text{RF}} \mathbf{F}_{\text{BB}}\|_F^2 &= P. \end{aligned} \quad (22)$$

In the following two subsections, we attempt to iteratively design the conditionally optimal analog beamformer and digital beamformer based on optimization problem (22).

B. FP-based Analog Beamformer Design

When \mathbf{r} , \mathbf{t} , and the digital beamformer \mathbf{F}_{BB} are fixed, the problem of conditionally optimal analog beamformer design can be presented as follows:

$$\begin{aligned} \mathbf{F}_{\text{RF}}^* &= \arg \max \delta \\ \text{s.t. } \mathbf{F}_{\text{RF}}(i, j) &\in \{0, \mathcal{F}\}, \forall i, j, \\ \|\mathbf{F}_{\text{RF}}(i, :)\|_0 &= 1, \forall i. \end{aligned} \quad (23)$$

In this analog beamformer design problem, we can ignore the power constraint since the digital beamformer can be adjusted to satisfy the power constraint. However, this problem is still difficult to be solved due to the discrete phase values and the l_0 norm constraint on the analog beamformer. In an effort to seek an available solution, we first rewrite the analog beamformer in the following form

$$\mathbf{F}_{\text{RF}} \triangleq \mathbf{S} \mathbf{F}_{\text{set}}, \quad (24)$$

where \mathbf{F}_{set} is defined as

$$\mathbf{F}_{\text{set}} \triangleq \begin{bmatrix} \mathbf{f}_{\text{set}} & \mathbf{0} & \dots & \mathbf{0} \\ \mathbf{0} & \mathbf{f}_{\text{set}} & & \mathbf{0} \\ \vdots & & \ddots & \vdots \\ \mathbf{0} & \mathbf{0} & \dots & \mathbf{f}_{\text{set}} \end{bmatrix}_{N_{\text{RF}}2^B \times N_{\text{RF}}} \quad (25)$$

with

$$\mathbf{f}_{\text{set}} \triangleq \frac{1}{\sqrt{N_t}} \left[1, e^{j\frac{2\pi}{2^B}}, \dots, e^{j\frac{2\pi(2^B-1)}{2^B}} \right]^T, \quad (26)$$

which contains all possible phases of a PS. $\mathbf{S} \in \{0, 1\}^{N_t \times N_{\text{RF}}2^B}$ is a binary matrix and $\mathbf{S}(i, j) = 1$ indicates that the i -th antenna is mapped to the $\lceil j/2^B \rceil$ -th RF chain with corresponding value $\mathbf{F}_{\text{set}}(j, \lceil j/2^B \rceil)$, where $\lceil \cdot \rceil$ denotes the ceiling operation. Therefore, with known \mathbf{F}_{set} , the analog beamformer design problem can be reformulated as

$$\begin{aligned} \mathbf{S}^* &= \arg \max \delta \\ \text{s.t. } & \|\mathbf{S}(i, :)\|_0 = 1, \forall i, \\ & \mathbf{S}(i, j) \in \{0, 1\}, \forall i, j. \end{aligned} \quad (27)$$

The optimization problem (27) is a typical 0/1 integer programming problem. Although it is still non-convex due to the discrete values of \mathbf{S} , the optimal \mathbf{S}^* can be found by some off-the-shelf solvers (e.g. Mosek optimization tools) using Branch and Bound methods [43], and then the corresponding optimal analog beamformer \mathbf{F}_{RF}^* can be obtained by

$$\mathbf{F}_{\text{RF}}^* = \mathbf{S}^* \mathbf{F}_{\text{set}}. \quad (28)$$

C. FP-based Digital Beamformer Design

With given \mathbf{r}, \mathbf{t} , and analog beamformer \mathbf{F}_{RF} , the problem of the conditionally optimal digital beamformer design can be expressed as:

$$\begin{aligned} \mathbf{F}_{\text{BB}}^* &= \arg \max \delta \\ \text{s.t. } & \|\mathbf{F}_{\text{RF}} \mathbf{F}_{\text{BB}}\|_F^2 = P. \end{aligned} \quad (29)$$

The optimal solution of problem (29) can be determined by Lagrangian multiplier method. By introducing a multiplier μ for the power constraint in (29), we can form a Lagrangian function as

$$L_\delta = \delta + \mu(P - \|\mathbf{F}_{\text{RF}} \mathbf{F}_{\text{BB}}\|_F^2) = \delta + \mu \left(P - \sum_{k=1}^K \|\mathbf{F}_{\text{RF}} \mathbf{f}_{\text{BB},k}\|_2^2 \right). \quad (30)$$

Therefore, the problem (29) can be reformulated as

$$\{\mathbf{F}_{\text{BB}}^*, \mu^*\} = \arg \max L_\delta. \quad (31)$$

Then the optimal solution of each row of \mathbf{F}_{BB} can be determined by setting the partial derivative of L_δ with respect to $\mathbf{f}_{\text{BB},k}$ and μ to zero, i.e.

$$\begin{cases} \frac{\partial L_\delta}{\partial \mathbf{f}_{\text{BB},k}} = \mathbf{0}, \forall k, \\ \frac{\partial L_\delta}{\partial \mu} = 0, \end{cases} \quad (32)$$

which yields the optimal digital beamformer as

$$\mathbf{f}_{\text{BB},k}^* = (\mathbf{A} + \mu^* \mathbf{F}_{\text{RF}}^H \mathbf{F}_{\text{RF}})^{-1} \sqrt{(1 + r_k)} \mathbf{F}_{\text{RF}}^H \mathbf{h}_k t_k, \forall k, \quad (33)$$

where the optimal multiplier μ^* is introduced for the power constraint and can be easily obtained by bisection search.

After having the methods to find the conditionally optimal auxiliary vectors \mathbf{r}^* and \mathbf{t}^* , digital beamformer \mathbf{F}_{BB}^* and analog beamformer \mathbf{F}_{RF}^* , the overall procedure of the proposed hybrid beamformer design is straightforward. With appropriate initial \mathbf{F}_{RF} and \mathbf{F}_{BB} , we iteratively update \mathbf{r} , \mathbf{t} , \mathbf{F}_{RF} , and \mathbf{F}_{BB} , until the convergence is observed. For clarity, the proposed FP-based hybrid beamformer design algorithm is summarized in Algorithm 1.

Algorithm 1 FP-Based Hybrid Beamformer Design Algorithm

Input: $\mathbf{h}_1, \dots, \mathbf{h}_k, B, N_t, N_{\text{RF}}, K$.

Output: $\mathbf{F}_{\text{RF}}^*, \mathbf{F}_{\text{BB}}^*$.

- 1: Initialize \mathbf{F}_{RF} and \mathbf{F}_{BB} .
 - 2: **while** no convergence of \mathbf{F}_{RF} and \mathbf{F}_{BB} **do**
 - 3: Update \mathbf{r}^* by (11).
 - 4: Update \mathbf{t}^* by (14).
 - 5: Update \mathbf{F}_{RF}^* by solving problem (27) to obtain binary matrix \mathbf{S}^* and constructing as (28).
 - 6: Update \mathbf{F}_{BB}^* by (33).
 - 7: **end while**
 - 8: Return \mathbf{F}_{RF}^* and \mathbf{F}_{BB}^* .
-

D. Convergence Analysis

In this subsection, we will provide the proof of convergence of the proposed FP-based hybrid precoder design algorithm. We start with introducing two inequations in the following proposition, which will be the foundation of the proof.

Proposition 3. Let $R(\mathbf{F}_{\text{RF}}, \mathbf{F}_{\text{BB}})$ be the sum-rate (7) as a function of beamformers \mathbf{F}_{RF} and \mathbf{F}_{BB} , $f_r(\mathbf{F}_{\text{RF}}, \mathbf{F}_{\text{BB}}, \mathbf{r})$ be the transformed objective function (10) by Proposition 1. Then, we will have

$$R(\mathbf{F}_{\text{RF}}, \mathbf{F}_{\text{BB}}) \geq f_r(\mathbf{F}_{\text{RF}}, \mathbf{F}_{\text{BB}}, \mathbf{r}), \quad (34)$$

where the equality holds if and only if each element of \mathbf{r} satisfies (11). Similarly, let $f_q(\mathbf{F}_{\text{RF}}, \mathbf{F}_{\text{BB}}, \mathbf{r}, \mathbf{t})$ be the transformed objective function (16) by Proposition 2. Then, we will have

$$f_r(\mathbf{F}_{\text{RF}}, \mathbf{F}_{\text{BB}}, \mathbf{r}) \geq f_q(\mathbf{F}_{\text{RF}}, \mathbf{F}_{\text{BB}}, \mathbf{r}, \mathbf{t}), \quad (35)$$

where the equality holds if and only if each element of \mathbf{t} satisfies (14).

Proof. These two inequations are straightforward since the values of \mathbf{r} in (11) and \mathbf{t} in (14) are all global optimal when the other variables are fixed. ■

Let $\mathbf{F}_{\text{RF}}^{(n)}$, $\mathbf{F}_{\text{BB}}^{(n)}$, $\mathbf{r}^{(n)}$, and $\mathbf{t}^{(n)}$ be the solutions of the n -th iteration obtained by Sec. III-A, (33), (11), and (14), respectively. According to the iterative procedure of Algorithm 1, we emphasize that $\mathbf{r}^{(n)}$ is obtained by (11) using beamformers of the n -th iteration (i.e. $\mathbf{F}_{\text{RF}}^{(n)}$, $\mathbf{F}_{\text{BB}}^{(n)}$) and $\mathbf{t}^{(n)}$ is obtained by (14) with respect to beamformers and \mathbf{r} of the n -th iteration (i.e. $\mathbf{F}_{\text{RF}}^{(n)}$, $\mathbf{F}_{\text{BB}}^{(n)}$, and $\mathbf{r}^{(n)}$). Moreover, we define $\mathbf{t}^{(n+1,n)}$ as the result obtained by (14) based on the beamformers of the $(n+1)$ -th iteration, but \mathbf{r} of the n -th iteration (i.e. $\mathbf{F}_{\text{RF}}^{(n+1)}$, $\mathbf{F}_{\text{BB}}^{(n+1)}$, and $\mathbf{r}^{(n)}$). Then by Proposition 3, we have

$$\begin{aligned} R(\mathbf{F}_{\text{RF}}^{(n+1)}, \mathbf{F}_{\text{BB}}^{(n+1)}) &= f_r(\mathbf{F}_{\text{RF}}^{(n+1)}, \mathbf{F}_{\text{BB}}^{(n+1)}, \mathbf{r}^{(n+1)}) \geq f_r(\mathbf{F}_{\text{RF}}^{(n+1)}, \mathbf{F}_{\text{BB}}^{(n+1)}, \mathbf{r}^{(n)}) \\ &= f_q(\mathbf{F}_{\text{RF}}^{(n+1)}, \mathbf{F}_{\text{BB}}^{(n+1)}, \mathbf{r}^{(n)}, \mathbf{t}^{(n+1,n)}) \geq f_q(\mathbf{F}_{\text{RF}}^{(n+1)}, \mathbf{F}_{\text{BB}}^{(n+1)}, \mathbf{r}^{(n)}, \mathbf{t}^{(n)}). \end{aligned} \quad (36)$$

Assume $\mathbf{F}_{\text{RF}}^{(n+1)}$ is the optimal solution using digital beamformer and two auxiliary vectors \mathbf{r} , \mathbf{t} of the n -th iteration (i.e. $\mathbf{F}_{\text{BB}}^{(n)}$, $\mathbf{r}^{(n)}$, and $\mathbf{t}^{(n)}$). Similarly, set $\mathbf{F}_{\text{BB}}^{(n+1)}$ as the optimal solution with analog beamformer of the $(n+1)$ -th iteration but \mathbf{r} , \mathbf{t} of the n -th iteration (i.e. $\mathbf{F}_{\text{RF}}^{(n+1)}$, and $\mathbf{r}^{(n)}, \mathbf{t}^{(n)}$). We further have

$$f_q(\mathbf{F}_{\text{RF}}^{(n+1)}, \mathbf{F}_{\text{BB}}^{(n+1)}, \mathbf{r}^{(n)}, \mathbf{t}^{(n)}) \geq f_q(\mathbf{F}_{\text{RF}}^{(n+1)}, \mathbf{F}_{\text{BB}}^{(n)}, \mathbf{r}^{(n)}, \mathbf{t}^{(n)}) \geq f_q(\mathbf{F}_{\text{RF}}^{(n)}, \mathbf{F}_{\text{BB}}^{(n)}, \mathbf{r}^{(n)}, \mathbf{t}^{(n)}). \quad (37)$$

Still by Proposition 3, we have

$$f_q(\mathbf{F}_{\text{RF}}^{(n)}, \mathbf{F}_{\text{BB}}^{(n)}, \mathbf{r}^{(n)}, \mathbf{t}^{(n)}) = f_r(\mathbf{F}_{\text{RF}}^{(n)}, \mathbf{F}_{\text{BB}}^{(n)}, \mathbf{r}^{(n)}) = R(\mathbf{F}_{\text{RF}}^{(n)}, \mathbf{F}_{\text{BB}}^{(n)}). \quad (38)$$

Therefore, we can conclude that the sum-rate objective is monotonically non-decreasing after each iteration, i.e.

$$R(\mathbf{F}_{\text{RF}}^{(n+1)}, \mathbf{F}_{\text{BB}}^{(n+1)}) \geq R(\mathbf{F}_{\text{RF}}^{(n)}, \mathbf{F}_{\text{BB}}^{(n)}), \quad (39)$$

which guarantees the convergence of Algorithm 1. Moreover, simulation results in Section V also further verify the convergence. It is worth noting that the algorithm may finally converge to a local optimum of optimization problem (17).

E. Complexity Analysis

Finally, we provide a brief analysis of the time complexity of the proposed FP-based hybrid precoder design algorithm. As shown in Algorithm 1, steps 5 and 6 have dominant computational cost in the proposed approach. Particularly, in each iteration, finding the digital beamformer in step 6 requires about $\mathcal{O}(KN_{\text{RF}}^3)$ complexity, which is mainly caused by the matrix inversion operation. Computing the analog beamformer in step 5 needs to solve an $N_{\text{RF}}2^B$ -dimensional integer programming optimization problem with N_t variables by CVX, which has $\mathcal{O}(\sqrt{N_t N_{\text{RF}} 2^B} [(N_{\text{RF}} 2^B)^3 N_t^2 + (N_{\text{RF}} 2^B)^2 N_t^3])$ complexity [46]. As a result, the overall time complexity of the proposed algorithm is about $\mathcal{O}(N_{\text{iter}}(KN_{\text{RF}}^3 + (N_t N_{\text{RF}} 2^B)^{\frac{5}{2}}(N_{\text{RF}} 2^B + N_t)))$, where N_{iter} is the number of iterations. Obviously, with larger number of transmit antennas, there will be substantial growth of the complexity of this algorithm. Therefore, in the next section, we propose another simple heuristic joint analog and digital beamformer design algorithm to dramatically reduce the time complexity but maintain acceptable performance.

IV. HEURISTIC HYBRID BEAMFORMER DESIGN

Similar with the proposed FP-based method described in the previous section, we propose an iterative scheme to obtain the analog beamformer and digital beamformer. To reduce the complexity of solving the analog beamformer, we attempt to successively design each nonzero element of the analog beamformer when the digital beamformer \mathbf{F}_{BB} is fixed. Then, with the effective baseband channel, we solve the digital beamformer based on uplink-downlink duality.

A. Heuristic Analog Beamformer Design

For the analog beamformer design, we propose to directly consider the original objective when the digital beamformer is fixed. Since the transmit power constraint can be satisfied by adjusting the digital beamformer, this analog beamformer design problem can be formulated as

$$\begin{aligned}
 \mathbf{F}_{\text{RF}}^* &= \arg \max R \\
 \text{s.t. } \mathbf{F}_{\text{RF}}(i, j) &\in \{0, \mathcal{F}\}, \forall i, j, \\
 \|\mathbf{F}_{\text{RF}}(i, :)\|_0 &= 1, \forall i.
 \end{aligned} \tag{40}$$

This problem is difficult to solve due to the complicated form of the objective function and non-convex constraints of the analog beamformer. However, from the l_0 norm constraint we can learn there is only one nonzero element in each row of the analog beamformer, which means that the analog beamformer matrix is sparse. This fact motivates us to sequentially consider the design for each nonzero element (i.e. each row) of the analog beamformer.

Given an initial value of analog beamformer \mathbf{F}_{RF} , we aim to successively update each row of the analog beamformer. Particularly, for the design of i -th row of the analog beamformer, $i = 1, \dots, N_t$, we attempt to conditionally increase the sum-rate performance R with fixed other rows of \mathbf{F}_{RF} , which can be expressed as

$$\mathbf{F}_{\text{RF}} = \underbrace{[\mathbf{F}_{\text{RF}}(1, :)^T, \dots, \mathbf{F}_{\text{RF}}(i-1, :)^T]}_{\text{fixed}}, \underbrace{\mathbf{F}_{\text{RF}}(i, :)^T}_{\text{to be updated}}, \underbrace{[\mathbf{F}_{\text{RF}}(i+1, :)^T, \dots, \mathbf{F}_{\text{RF}}(N_t, :)^T]}_{\text{fixed}}^T. \tag{41}$$

Therefore, the sub-problem to determine the i -th row of the analog beamformer can be expressed as

$$\begin{aligned}
 \mathbf{F}_{\text{RF}}^*(i, :) &= \arg \max_{\mathbf{F}_{\text{RF}}(i, :)} R \\
 \text{s.t. } \mathbf{F}_{\text{RF}}(i, j) &\in \{\mathcal{F}, 0\}, \forall j, \\
 \|\mathbf{F}_{\text{RF}}(i, :)\|_0 &= 1.
 \end{aligned} \tag{42}$$

Benefiting from using low-resolution PSs, we can perform a low-complexity two-dimensional exhaustive search over N_{RF} RF chains and \mathcal{F} with $|\mathcal{F}| = 2^B$, which only requires complexity of $\mathcal{O}(N_{\text{RF}}2^B)$. By successively solving the subproblem (42) over all the transmit antennas (i.e. rows of \mathbf{F}_{RF}), the analog beamformer can be obtained.

B. Digital Beamformer Design Based on Uplink-downlink Duality

When the analog beamformer is determined, we can obtain the effective baseband channel $\tilde{\mathbf{h}}_k, k = 1, \dots, K$, for each user as

$$\tilde{\mathbf{h}}_k^H \triangleq \mathbf{h}_k^H \mathbf{F}_{\text{RF}}^*. \quad (43)$$

Then, the digital beamformer should be designed based on the effective baseband channel to further enhance the sum-rate performance. Similar problems have been intensively investigated for conventional fully-digital beamforming schemes. Therefore, in this paper, we adopted classic uplink-downlink duality theorem [44] and cyclic self-SINR-maximization (CSSM) algorithm [45] to solve the digital beamformer design problem. The procedure is briefly described below.

Based on the theory of uplink-downlink SINR duality, the original downlink beamformer design problem can be solved by solving its dual uplink optimization problem first, which is given by

$$\begin{aligned} \{\mathbf{f}_1, \dots, \mathbf{f}_K, q_1, \dots, q_K\} &= \arg \max \sum_{k=1}^K \log(1 + \text{SINR}_k^{\text{ul}}) \\ \text{s.t. } &\mathbf{f}_k^H \mathbf{f}_k = 1, \forall k, \\ &\sum_{k=1}^K q_k \leq P, \end{aligned} \quad (44)$$

where

$$\text{SINR}_k^{\text{ul}} = \frac{q_k \mathbf{f}_k^H \tilde{\mathbf{h}}_k \tilde{\mathbf{h}}_k^H \mathbf{f}_k}{\mathbf{f}_k^H (\sum_{j \neq k} q_j \tilde{\mathbf{h}}_j \tilde{\mathbf{h}}_j^H) \mathbf{f}_k + \sigma_k^2}, k = 1, \dots, K, \quad (45)$$

is the dual uplink SINR for the k -th user, $\mathbf{f}_k, k = 1, \dots, K$, are the normalized digital beamformer vectors and $q_k, k = 1, \dots, K$, are uplink powers. Applying the CSSM algorithm, the dual uplink optimization problem (44) can be solved by the following iterative procedure:

Step 1: Obtain the max-SINR beamformer vectors $\mathbf{f}_k, k = 1, \dots, K$, as

$$\mathbf{f}_k = \left(\sum_{j=1, j \neq k}^K q_j \tilde{\mathbf{h}}_j \tilde{\mathbf{h}}_j^H + \sigma_k^2 \mathbf{I} \right)^{-1} \tilde{\mathbf{h}}_k, \forall k, \quad (46)$$

each of which is further normalized by

$$\mathbf{f}_k = \frac{\mathbf{f}_k}{\|\mathbf{f}_k\|}, \forall k. \quad (47)$$

Step 2: Adjust powers q_k with water-filling algorithm as

$$q_k = \left(\frac{1}{\mu} - \frac{1}{\varepsilon_k} \right)^+, \forall k, \quad (48)$$

where $\varepsilon_k \triangleq \tilde{\mathbf{h}}_k^H (\sum_{j \neq k} q_j \tilde{\mathbf{h}}_j \tilde{\mathbf{h}}_j^H + \sigma_k^2 \mathbf{I})^{-1} \tilde{\mathbf{h}}_k$, μ satisfies the power constraint, $(x)^+ = \max\{x, 0\}$.

Step 3: Alternatively update the beamformer vectors and powers until the stop criterion is satisfied (i.e. the difference of total power $\sum_{k=1}^K q_k$ between two consecutive iterations is smaller than a given threshold).

Given the optimal digital beamformer vectors and powers for the dual uplink problem, the original downlink problem can be easily solved. Based on the uplink-downlink duality, with the same beamformer vectors and power constraint, the downlink system can achieve the same SINRs as the uplink case by using the downlink powers $p_k, k = 1, \dots, K$, as

$$p_k = \sum_{i=1}^K (\mathbf{B}^T)^{-1}(k, i), \forall k, \quad (49)$$

where \mathbf{B} is a $K \times K$ matrix and

$$\mathbf{B}(i, j) = \begin{cases} -|\tilde{\mathbf{h}}_i^H \mathbf{f}_j|^2, & i \neq j, \\ |\tilde{\mathbf{h}}_i^H \mathbf{f}_i| / \text{SINR}_i^{\text{ul}}, & i = j. \end{cases} \quad (50)$$

Thus, the energy-included digital beamformer for original downlink system can be given by

$$\hat{\mathbf{f}}_{\text{BB},k} = \sqrt{p_k} \mathbf{f}_k, \forall k. \quad (51)$$

To guarantee the power constraint, the final digital beamformer is normalized by

$$\mathbf{F}_{\text{BB}}^* = \frac{\sqrt{P} \hat{\mathbf{F}}_{\text{BB}}}{\|\mathbf{F}_{\text{RF}} \hat{\mathbf{F}}_{\text{BB}}\|_F}. \quad (52)$$

where $\hat{\mathbf{F}}_{\text{BB}} = [\hat{\mathbf{f}}_{\text{BB},1}, \dots, \hat{\mathbf{f}}_{\text{BB},K}]$.

Based on the description in Sec. IV-A and Sec. IV-B, the iterative procedure of hybrid beamformer design is now straightforward. After selecting appropriate initial \mathbf{F}_{RF} and \mathbf{F}_{BB} , we propose to iteratively update the analog beamformer and the digital beamformer until the convergence is satisfied. The complete procedure for this heuristic hybrid beamformer design algorithm is summarized in Algorithm 2.

C. Complexity Analysis

We also give a brief complexity analysis of the proposed heuristic hybrid beamformer design algorithm. In each updating step, running through a full iteration over all N_t antennas (i.e. N_t rows of \mathbf{F}_{RF}) to obtain the analog beamformer requires $\mathcal{O}(N_t^2 N_{\text{RF}}^3 2^B)$. Calculating the digital beamformer requires $\mathcal{O}(N_1 K N_{\text{RF}}^3)$,

Algorithm 2 Heuristic Hybrid Beamformer Design

Input: $\mathbf{h}_1, \dots, \mathbf{h}_K, B, N_t, N_{\text{RF}}, K$.**Output:** $\mathbf{F}_{\text{RF}}^*, \mathbf{F}_{\text{BB}}^*$.

```
1: Initialize  $\mathbf{F}_{\text{RF}}, \mathbf{F}_{\text{BB}}$ .
2: while no convergence of  $\mathbf{F}_{\text{RF}}$  and  $\mathbf{F}_{\text{BB}}$  do
3:   Analog beamformer design:
4:   for  $i = 1 : N_t$  do
5:     Update  $\mathbf{F}_{\text{RF}}(i, :)$  by solving problem (42).
6:   end for
7:   Digital beamformer design:
8:   while no convergence of  $\mathbf{f}_k$  and  $q_k, \forall k$  do
9:     for  $k = 1, \dots, K$  do
10:      Update uplink beamformer  $\mathbf{f}_k$  as (46) and (47).
11:    end for
12:    for  $k = 1, \dots, K$  do
13:      Update uplink power  $q_k$  as (48).
14:    end for
15:  end while
16:  Compute downlink beamformer  $\mathbf{F}_{\text{BB}}$  by (49)-(51).
17:  Normalize  $\mathbf{F}_{\text{BB}}$  as (52).
18: end while
19: Return  $\mathbf{F}_{\text{RF}}$  and  $\mathbf{F}_{\text{BB}}$ .
```

where N_1 denotes the number of iterations for CSSM algorithm. As a result, the overall complexity of the proposed algorithm is $\mathcal{O}(N_{\text{iter}}(N_t^2 N_{\text{RF}}^3 2^B + N_1 K N_{\text{RF}}^3))$, where N_{iter} is the number of iterations for the proposed algorithm.

Now, we turn to compare the complexities of two proposed algorithms. When the number of transmit antennas N_t is much larger than the number of users K and RF chains N_{RF} , which is usually the case, the complexity of the FP-based hybrid beamformer design algorithm can be simplified as

$$C_{\text{FP}} = \mathcal{O}(N_{\text{iter}} N_t^{\frac{7}{2}} (N_{\text{RF}} 2^B)^{\frac{5}{2}}). \quad (53)$$

Similarly, the complexity of the heuristic hybrid beamformer design algorithm can be given by

$$C_{\text{Heuristic}} = \mathcal{O}(N_{\text{iter}} N_t^2 N_{\text{RF}}^3 2^B). \quad (54)$$

Therefore, we can draw a conclusion that the latter algorithm can significantly reduce the complexity especially when the large-scale antenna array is adopted. Moreover, simulation results in the next section indicate that the latter algorithm has faster convergence speed than the former scheme, which further strengthens our conclusion.

V. SIMULATION RESULTS

In this section, we present simulation results to demonstrate the sum-rate and energy efficiency (EE) performance of two proposed hybrid beamformer designs with dynamic subarrays and low-resolution PSs. In the considered MU-MISO system, the BS is equipped with totally $N_t = N_x \times N_y = 6 \times 6 = 36$ antennas and $N_{\text{RF}} = 3$ RF chains, where antenna spacing d is $\lambda/2$ and λ denotes the wavelength. Without loss of generality, we assume the number of users K is equal to the number of RF chains, i.e. $N_{\text{RF}} = K$. In the simulation, the channel parameter is set as $L = 5$ paths. Furthermore, horizontal and vertical AoDs are uniformly distributed over $[-\frac{\pi}{2}, \frac{\pi}{2}]$ and $[-\frac{\pi}{4}, \frac{\pi}{4}]$, respectively. The signal-to-noise-ratio (SNR) is defined as $\frac{P}{\sigma_k^2}$ with $\sigma_k^2 = 1, k = 1, \dots, K$. Finally, simulation results are averaged over 10^5 channel realizations.

A. Sum-rate Performance

In Fig. 3, we first present the convergence of two proposed hybrid beamformer designs by plotting the sum-rate performance versus the number of iterations. The SNR is fixed as 10dB. Simulation results illustrate that the convergence of both two algorithms is really fast. Specifically, the FP-based hybrid beamformer design algorithm will converge within 8 iterations while the heuristic design algorithm has convergence within 4 iterations. The convergence speed of the proposed two algorithms also indicates that the heuristic algorithm can effectively reduce the time complexity compared with the FP-based hybrid beamformer design algorithm even when a larger antenna array is used. From Fig. 3, we can also notice that the FP-based algorithm has better performance. Moreover, with the growth of the resolution of PSs, the proposed two algorithms both tend to achieve better sum-rate performance.

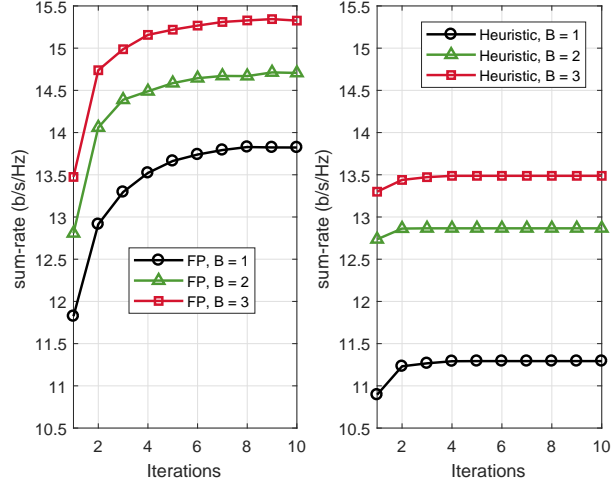


Fig. 3. The convergence of the proposed algorithms: Left: FP-based algorithm; Right: Heuristic algorithm (number of total antennas $N_t = 6 \times 6 = 36$, number of users $K = 3$, SNR = 10dB).

Fig. 4 shows the achievable sum-rate versus SNR, in which we demonstrate the performance of two proposed hybrid beamformer design algorithms for the cases of using $B = 1, 2$ -bit resolution PSs. For the comparison purpose, we also include four algorithms: *i*) Traditional fully-digital (**FD**) beamforming [45]; *ii*) fully-connected (**FC**) hybrid beamforming [25] for the case of using $B = 2$ bit and $B = \infty$ bit resolution PSs; *iii*) dynamic subarray hybrid beamforming with double infinite-resolution PSs (**DS**, **DPS**) [33]; *iv*) fixed-subarray (**FS**) hybrid beamforming with successive interference cancelation (SIC) based beamformer design [19]. Since the original SIC-based beamformer design algorithm was developed for the infinite-resolution PS case, for the fair comparison purpose, we directly quantize the result of the analog beamformer to low-resolution values. It can be observed from Fig. 4 that the FP-based algorithm always achieves better performance than the heuristic scheme in different SNR ranges. Specifically when $B = 2$, the FP-based algorithm can achieve satisfactory performance close to dynamic subarray scheme with double infinite-resolution PSs, which can serve as the performance upper bound of our algorithm because of the use of finer and more PSs. More importantly, the proposed two hybrid beamforming solutions with dynamic subarrays and low-resolution PSs both can notably outperform the conventional fixed-subarray architecture.

In Fig. 5, we show the sum-rates of two proposed algorithms with respect to the number of antennas N_t . In this case, we fix the number of users as $K = 3$ and SNR = 10dB. A similar conclusion can be drawn from Fig. 5 that the proposed algorithms both achieve superior performance compared with fixed-

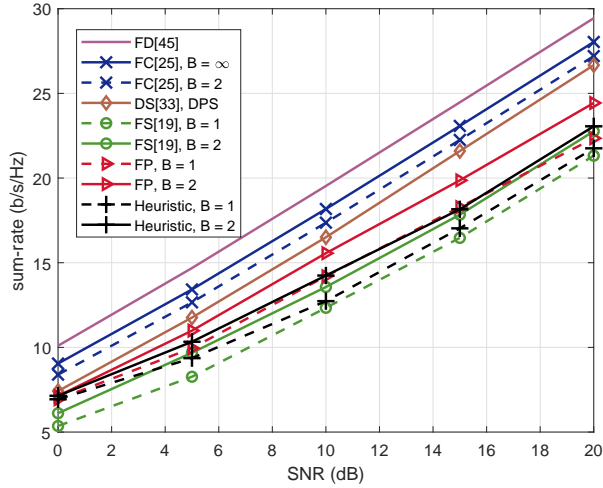


Fig. 4. Sum-rate versus SNR (number of total transmit antennas $N_t = 6 \times 6 = 36$, number of users $K = 3$).

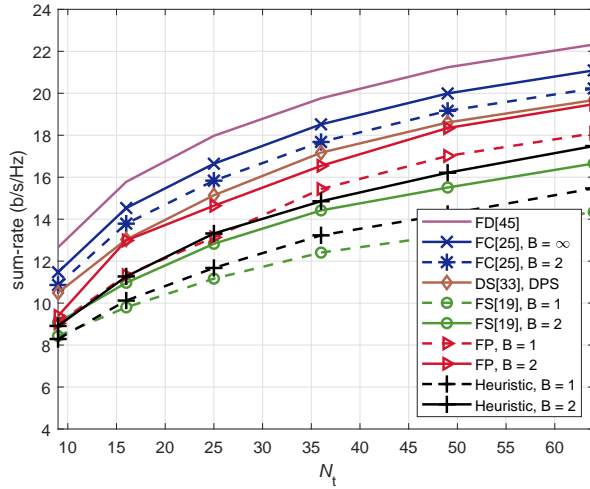


Fig. 5. Sum-rate versus number of total transmit antennas (number of users $K = 3$, SNR = 10dB).

subarray schemes. We can also expect that the sum-rate performance will become better as the increase of the number of antennas N_t , which can offer more antenna diversity and beamforming gain.

In Fig. 6, we illustrate the average sum-rate as a function of the number of users with the fixed number of antennas $N_t = 36$ and SNR = 10dB. It further verifies that both two proposed algorithms always outperform fixed-subarray schemes with different user populations. Furthermore, with the growth of the number of users, the performance gap between the fully-digital beamforming architecture and subarray schemes will become larger. This phenomenon reveals an interesting fact: When the number of transmit antennas is fixed, serving more users will induce more multiuser diversity, but in the meanwhile, make it more difficult to eliminate the inter-user interference due to the less number of antennas in each subarray/user. Therefore,

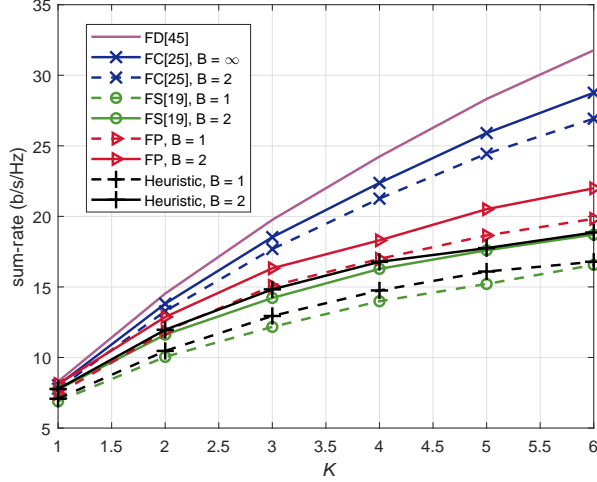


Fig. 6. Sum-rate versus number of users (number of total transmit antennas $N_t = 6 \times 6 = 36$, SNR = 10dB).

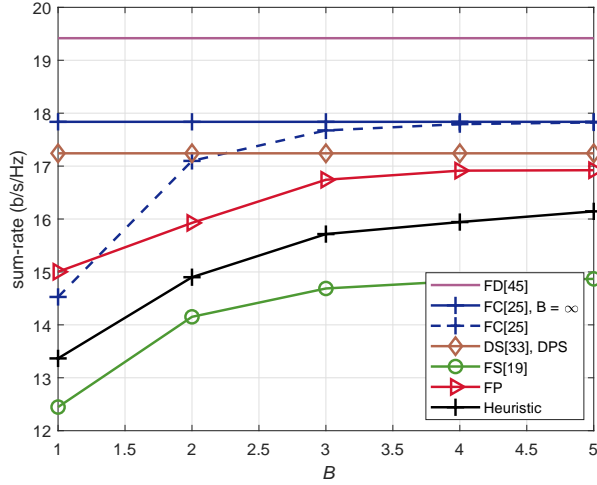


Fig. 7. Sum-rate versus the resolution of PSs (number of total antennas $N_t = 6 \times 6 = 36$, number of users $K = 3$, SNR = 10dB).

it is important to properly set numbers of antennas and users for subarray schemes.

Fig. 7 shows the sum-rate performance as a function of B to illustrate the influence of the resolution of PSs on the system performance. It can be clearly observed from Fig. 7 that the sum-rate performance will first increase and then tend to saturate with the growth of B . When $B = 4$, the performance achieved by the FP-based algorithm can approach that of dynamic subarray scheme with double infinite-resolution PSs, this result confirms that the low-resolution PSs are practical and sufficient for the real-world hybrid beamforming schemes.

B. EE Performance

In an effort to find the tradeoff between sum-rate performance and energy consumption, we illustrate the EE of the proposed designs, which is defined as

TABLE I
POWER CONSUMPTIONS FOR DIFFERENT DEVICES IN MMWAVE SYSTEMS

Hardware Device	Power Consumption (mW)
Baseband processor	$P_{\text{BB}} = 200$
RF chain	$P_{\text{RF}} = 300$ [27]
PS	$P_{\text{PS}} = 10 (B = 1)$ $P_{\text{PS}} = 20 (B = 2)$ [39]
SW	$P_{\text{SW}} = 5$ [27]

$$\eta \triangleq \frac{R}{P_{\text{tot}}}, \quad (55)$$

where P_{tot} is the total power consumption of the BS. For the fully-digital beamforming architecture, the total power consumption is defined as

$$P_{\text{tot}}^{\text{FD}} \triangleq P + P_{\text{BB}} + N_{\text{t}}P_{\text{RF}}, \quad (56)$$

where P is the transmit power, P_{BB} and P_{RF} are the powers consumed by the baseband processor and a RF chain, respectively. For fully-connected hybrid beamforming architecture, the total power consumption can be introduced as

$$P_{\text{tot}}^{\text{FC}} \triangleq P + P_{\text{BB}} + N_{\text{RF}}P_{\text{RF}} + N_{\text{t}}N_{\text{RF}}P_{\text{PS}}, \quad (57)$$

where P_{PS} is the energy consumed by a PS. For traditional fixed-subarray schemes, the total power consumption is given by

$$P_{\text{tot}}^{\text{FS}} \triangleq P + P_{\text{BB}} + N_{\text{RF}}P_{\text{RF}} + N_{\text{t}}P_{\text{PS}}. \quad (58)$$

Finally, for the proposed dynamic subarray scheme, the total power consumption can be written as

$$P_{\text{tot}}^{\text{DS}} \triangleq P + P_{\text{BB}} + N_{\text{RF}}P_{\text{RF}} + N_{\text{t}}P_{\text{PS}} + N_{\text{t}}P_{\text{SW}}, \quad (59)$$

where P_{SW} is the energy consumed by a SW. In this simulation, the power consumptions of different devices in practical mmWave systems are listed in Table I.

In Fig. 8, we present EE performance as a function of the number of transmit antennas N_{t} . It can be observed in Fig. 8 that the proposed FP-based hybrid beamformer design algorithm can maintain the best EE performance with the growing number of antennas. Unfortunately, the EE achieved by the heuristic

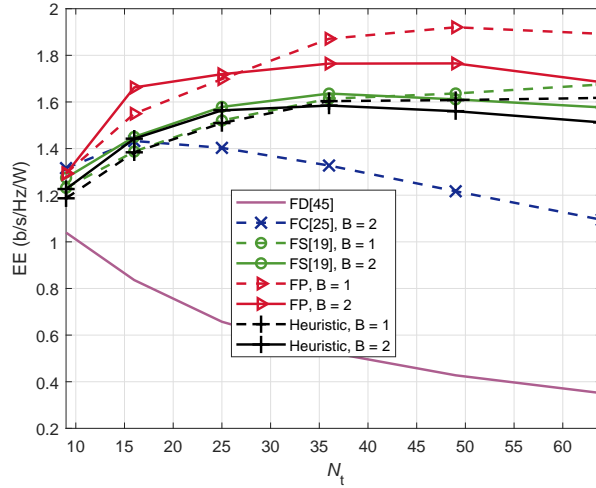


Fig. 8. EE versus number of total antennas N_t . (number of users $K = 3$, $P = 1W$).

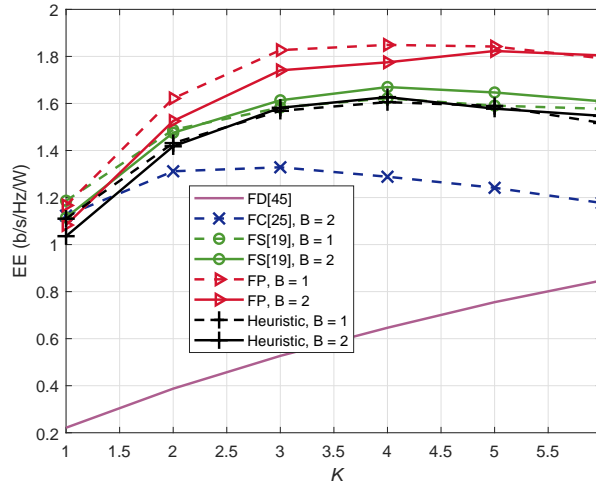


Fig. 9. EE versus K (number of total transmit antennas $N_t = 6 \times 6 = 36$, number of RF chains $N_{RF} = K$).

hybrid beamformer design algorithm is a little lower than the fixed-subarray scheme. This is because that, even though the heuristic hybrid beamformer design has better sum-rate performance, it also requires an additional SW network to implement dynamic subarrays, which will consume more energy than the fixed-subarray scheme. Then in Fig. 9, we further simulate the EE performance versus the number of users (i.e. number of RF chains). Similar conclusion as Fig. 8 can be drawn. Moreover, the EE performance does not always grow with the increasing of number of RF chains and four or five RF chains can provide the best EE performance.

Finally, Fig. 10 illustrates the EE performance versus SNR when the numbers of transmit antennas and users are fixed as $N_t = 36$ and $K = 3$, respectively. In this figure, the variance of the Gaussian

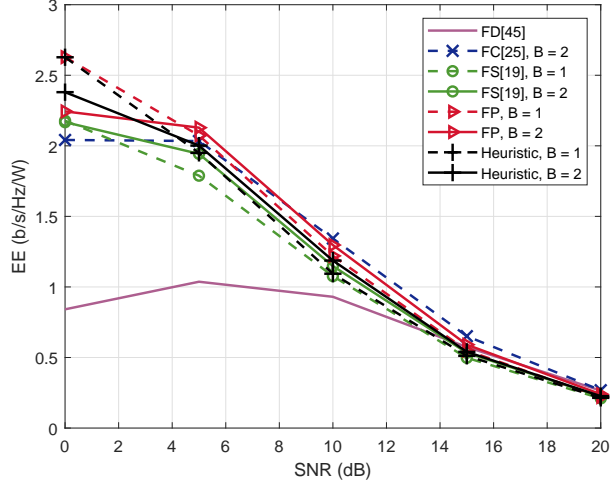


Fig. 10. EE versus SNR (number of total transmit antennas $N_t = 6 \times 6 = 36$, number of users $K = 3$).

noise is fixed as $\sigma_k^2 = 1, k = 1, \dots, K$, and the transmit power P is varying to simulate different SNR situations. The proposed two algorithms can always achieve satisfactory performance than their competitors. Moreover, with the growth of SNR, the EE gap among different schemes becomes smaller. The reason for this phenomenon is that the transmit power tends to dominate the total power consumption when SNR increases.

VI. CONCLUSIONS

In this paper, we introduced a novel efficient hybrid beamformer architecture with dynamic subarrays and low-resolution phase shifters (PSs) for a mmWave downlink multiuser multiple-input single-output (MU-MISO) system. Aiming at optimizing the system sum-rate performance, we first proposed an iterative hybrid beamformer design algorithm based on the theory of fractional programming (FP). In order to reduce the time complexity, we also proposed another heuristic hybrid beamformer design algorithm which has low complexity even when the number of antennas got large. The effectiveness of two proposed hybrid beamformer designs was validated by extensive simulation results, which illustrated that both two algorithms can remarkably outperform traditional fixed-subarray schemes. For the future studies, it would be interesting to extend the proposed hybrid beamformer architecture with dynamic subarrays and low-resolution PSs to multi-user/multi-stream MIMO systems and wideband systems.

APPENDIX A

Proof of Proposition 1: By introducing K auxiliary variables $r_k, k = 1, \dots, K$, to replace each ratio part (i.e. $\text{SINR}_k, k = 1, \dots, K$) of objective in (9), the unconstrained sum-rate maximization problem can

be rewritten as

$$\begin{aligned} \max \quad & \sum_{k=1}^K \log(1 + r_k) \\ \text{s.t.} \quad & r_k \leq \text{SINR}_k, \forall k. \end{aligned} \quad (60)$$

Obviously, (60) is a convex problem which can be easily solved by many optimization methods, e.g. Lagrangian multiplier method. By introducing K multipliers $\lambda_k, k = 1, \dots, K$, for each inequality constraint in (60), we can form a Lagrangian function as

$$L = \sum_{k=1}^K \log(1 + r_k) - \sum_{k=1}^K \lambda_k (r_k - \text{SINR}_k). \quad (61)$$

The optimal r_k^* and $\lambda_k^*, k = 1, \dots, K$, can be obtained by setting $\frac{\partial L}{\partial r_k} = 0$ and $\frac{\partial L}{\partial \lambda_k} = 0$:

$$r_k^* = \text{SINR}_k, \forall k, \quad (62)$$

$$\lambda_k^* = \frac{1}{1 + r_k^*}, \forall k. \quad (63)$$

With given r_k^* and λ_k^* in (62) and (63), the maximal value of (61) can be written as

$$L^* = \sum_{k=1}^K \log(1 + r_k^*) - \sum_{k=1}^K \frac{1}{1 + r_k^*} (r_k^* - \text{SINR}_k) \quad (64)$$

$$= \sum_{k=1}^K \log(1 + r_k^*) - \sum_{k=1}^K \frac{r_k^*}{1 + r_k^*} + \sum_{k=1}^K \frac{\text{SINR}_k}{1 + r_k^*} \quad (65)$$

$$= \sum_{k=1}^K \log(1 + r_k^*) - \sum_{k=1}^K \frac{r_k^* (\sum_{j \neq k} |\mathbf{h}_k^H \mathbf{F}_{\text{RF}} \mathbf{f}_{\text{BB},j}|^2 + \sigma_k^2)}{\sum_{j=1}^K |\mathbf{h}_k^H \mathbf{F}_{\text{RF}} \mathbf{f}_{\text{BB},j}|^2 + \sigma_k^2} + \sum_{k=1}^K \frac{|\mathbf{h}_k^H \mathbf{F}_{\text{RF}} \mathbf{f}_{\text{BB},k}|^2}{\sum_{j=1}^K |\mathbf{h}_k^H \mathbf{F}_{\text{RF}} \mathbf{f}_{\text{BB},j}|^2 + \sigma_k^2} \quad (66)$$

$$= \sum_{k=1}^K \log(1 + r_k^*) - \sum_{k=1}^K r_k^* + \sum_{k=1}^K \frac{|\mathbf{h}_k^H \mathbf{F}_{\text{RF}} \mathbf{f}_{\text{BB},k}|^2 (1 + r_k^*)}{\sum_{j=1}^K |\mathbf{h}_k^H \mathbf{F}_{\text{RF}} \mathbf{f}_{\text{BB},j}|^2 + \sigma_k^2}, \quad (67)$$

which has the same form as f_r in (10) in Proposition 1.

Conversely, when \mathbf{F}_{RF} and \mathbf{F}_{BB} are all fixed, it can be observed that (10) is a concave function of \mathbf{r} . Based on it, \mathbf{r} can be directly determined by setting $\frac{\partial f_r}{\partial r_k} = 0, k = 1, \dots, K$, i.e.

$$r_k^* = \text{SINR}_k = \frac{|\mathbf{h}_k^H \mathbf{F}_{\text{RF}} \mathbf{f}_{\text{BB},k}|^2}{\sum_{j \neq k} |\mathbf{h}_k^H \mathbf{F}_{\text{RF}} \mathbf{f}_{\text{BB},j}|^2 + \sigma_k^2}, \forall k. \quad (68)$$

Substituting the \mathbf{r}^* back into (10), the objective function (10) becomes that in (9) exactly, which completes the proof. ■

APPENDIX B

Proof of Proposition 2: The function (13) can be rewritten as:

$$\sqrt{1+r_k}(t_k^* \mathbf{h}_k^H \mathbf{F}_{\text{RF}} \mathbf{f}_{\text{BB},k} + \mathbf{f}_{\text{BB},k}^H \mathbf{F}_{\text{RF}}^H \mathbf{h}_k t_k) - |t_k|^2 \left(\sum_{j=1}^K |\mathbf{h}_k^H \mathbf{F}_{\text{RF}} \mathbf{f}_{\text{BB},j}|^2 + \sigma_k^2 \right) \quad (69)$$

$$= \left(\sum_{j=1}^K |\mathbf{h}_k^H \mathbf{F}_{\text{RF}} \mathbf{f}_{\text{BB},j}|^2 + \sigma_k^2 \right) \left(\frac{\sqrt{1+r_k}(t_k^* \mathbf{h}_k^H \mathbf{F}_{\text{RF}} \mathbf{f}_{\text{BB},k} + \mathbf{f}_{\text{BB},k}^H \mathbf{F}_{\text{RF}}^H \mathbf{h}_k t_k)}{\sum_{j=1}^K |\mathbf{h}_k^H \mathbf{F}_{\text{RF}} \mathbf{f}_{\text{BB},j}|^2 + \sigma_k^2} - |t_k|^2 \right) \quad (70)$$

$$= \left(\sum_{j=1}^K |\mathbf{h}_k^H \mathbf{F}_{\text{RF}} \mathbf{f}_{\text{BB},j}|^2 + \sigma_k^2 \right) \left(\frac{(1+r_k)|\mathbf{h}_k^H \mathbf{F}_{\text{RF}} \mathbf{f}_{\text{BB},k}|^2}{(\sum_{j=1}^K |\mathbf{h}_k^H \mathbf{F}_{\text{RF}} \mathbf{f}_{\text{BB},j}|^2 + \sigma_k^2)^2} - \left| \frac{\sqrt{1+r_k} \mathbf{h}_k^H \mathbf{F}_{\text{RF}} \mathbf{f}_{\text{BB},k}}{\sum_{j=1}^K |\mathbf{h}_k^H \mathbf{F}_{\text{RF}} \mathbf{f}_{\text{BB},j}|^2 + \sigma_k^2} - t_k \right|^2 \right). \quad (71)$$

It can be verified from (71) that when the last absolute-norm term of (71) equals to zero, i.e.

$$t_k^* = \frac{\sqrt{1+r_k} \mathbf{h}_k^H \mathbf{F}_{\text{RF}} \mathbf{f}_{\text{BB},k}}{\sum_{j=1}^K |\mathbf{h}_k^H \mathbf{F}_{\text{RF}} \mathbf{f}_{\text{BB},j}|^2 + \sigma_k^2}, \quad (72)$$

function (71) has the same form as (12) exactly. Proposition 2 is therefore proved. ■

REFERENCES

- [1] Z. Pi and F. Khan, "An introduction to millimeter-wave mobile broadband systems," *IEEE Commun. Mag.*, vol. 49, no. 6, pp. 101-107, June 2011.
- [2] T. Rappaport, S. Sun, R. Mayzus, H. Zhao, Y. Azar, K. Wang, G. N. Wong, J. K. Schulz, M. Samimi and F. Gutierrez "Millimeter wave mobile communications for 5G cellular: It will work!" *IEEE Access*, vol. 1, pp. 335-349, 2013.
- [3] A. Lee Swindlehurst, E. Ayanoglu, P. Heydari, and F. Capolino, "Millimeter-wave massive MIMO: The next wireless revolution?" *IEEE Commun. Mag.*, vol. 52, no. 9, pp. 56-62, Sept. 2014.
- [4] R. W. Heath Jr., N. González-Prelcic, S. Rangan, W. Roh, and A. M. Sayeed, "An overview of signal processing techniques for millimeter wave MIMO systems," *IEEE J. Sel. Topics Signal Process.*, vol. 10, no. 3, pp. 436-453, Apr. 2016.
- [5] A. Alkhateeb, J. Mo, N. González-Prelcic, and R. W. Heath, "MIMO precoding and combining for millimeter-wave systems," *IEEE Commun. Mag.*, vol. 52, no. 12, pp. 122-131, Dec. 2014.
- [6] A. S. Y. Poon and M. Taghivand, "Supporting and enabling circuits for antenna arrays in wireless communications," *Proc. IEEE*, vol. 100, no. 7, pp. 2207-2218, July 2012.
- [7] S. Han, C.-L. I, Z. Xu, and C. Rowell, "Large-scale antenna systems with hybrid analog and digital beamforming for millimeter wave 5G," *IEEE Commun. Mag.*, vol. 53, no. 1, pp. 186-194, Jan. 2015.
- [8] X. Yu, J.-C. Shen, J. Zhang, and K. B. Letaief, "Alternating minimization algorithms for hybrid precoding in millimeter wave MIMO systems," *IEEE J. Sel. Topics Signal Process.*, vol. 10, no. 3, pp. 485-500, Apr. 2016.
- [9] C. Rusu, R. Méndez-Rial, N. González-Prelcic, and R. W. Heath Jr., "Low complexity hybrid precoding strategies for millimeter wave communication systems," *IEEE Trans. Wireless Commun.*, vol. 15, no. 12, pp. 8380-8393, Sept. 2016.
- [10] W. Ni, X. Dong, and W.-S. Lu, "Near-optimal hybrid processing for massive MIMO systems via matrix decomposition," *IEEE Trans. Signal Process.*, vol. 65, no. 15, pp. 3922-3933, Aug. 2017.

- [11] O. E. Ayach, S. Rajagopal, S. Abu-Surra, Z. Pi, and R. W. Heath Jr., "Spatially sparse precoding in millimeter wave MIMO systems," *IEEE Trans. Wireless Commun.*, vol. 13, no. 3, pp. 1499-1513, Mar. 2014.
- [12] J. Zhang, Y. Huang, Q. Shi, J. Wang, and L. Yang, "Codebook Design for Beam Alignment in Millimeter Wave Communication Systems," *IEEE Trans. Commun.*, vol. 65, no. 11, pp. 4980-4995, Nov. 2017.
- [13] S. He, J. Wang, Y. Huang, B. Ottersten, and W. Hong, "Codebook-Based Hybrid Precoding for Millimeter Wave Multiuser Systems," *IEEE Trans. Signal Process.*, vol. 65, no. 20, pp. 5289-5304, Oct. 2017.
- [14] A. Li and C. Masouros, "Hybrid precoding and combining design for millimeter-wave multi-user MIMO based on SVD," in *Proc. IEEE Int. Conf. Commun. (ICC)*, Paris, France, May 2017, pp. 1-6.
- [15] W. Ni and X. Dong, "Hybrid block diagonalization for massive multiuser MIMO systems," *IEEE Trans. Commun.*, vol. 64, no. 1, pp. 201-211, Jan. 2016.
- [16] A. Alkhateeb, G. Leus, and R. W. Heath Jr., "Limited feedback hybrid precoding for multi-user millimeter wave systems," *IEEE Trans. Wireless Commun.*, vol. 14, no. 11, pp. 6481-6494, Nov. 2015.
- [17] Z. Wang, M. Li, X. Tian, and Q. Liu, "Iterative hybrid precoder and combiner design for mmWave multiuser MIMO systems," *IEEE Commun. Lett.*, vol. 21, no. 7, pp. 1581-1584, July 2017.
- [18] O. El Ayach, R. W. Heath Jr., S. Rajagopal, and Z. Pi, "Multimode precoding in millimeter wave MIMO transmitters with multiple antenna sub-arrays," in *Proc. IEEE Global Commun. Conf. (GLOBECOM)*, Atlanta, GA, Dec. 2013, pp. 3476-3480.
- [19] X. Gao, L. Dai, S. Han, C.-L. I, and R. W. Heath Jr., "Energy-efficient hybrid analog and digital precoding for mmWave MIMO systems with large antenna arrays," *IEEE J. Sel. Areas Commun.*, vol. 34, no. 4, pp. 998-1009, Apr. 2016.
- [20] S. He, C. Qi, Y. Wu, and Y. Huang, "Energy-efficient transceiver design for hybrid sub-array architecture MIMO systems," *IEEE Access*, vol. 4, pp. 9895-9905, 2016.
- [21] W. Huang, Z. Lu, Y. Huang and L. Yang, "Hybrid precoding for single carrier wideband multi-subarray millimeter wave systems," *IEEE Wireless Commun. Lett.*, to appear, doi: 10.1109/LWC.2018.2877358.
- [22] M. Li, Z. Wang, H. Li, Q. Liu, and L. Zhou, "A hardware-efficient hybrid beamforming solution for mmWave MIMO systems," *IEEE Wireless Commun.*, to appear.
- [23] F. Sotrobiani and W. Yu, "Hybrid digital and analog beamforming design for large-scale antenna arrays," *IEEE J. Sel. Topics Signal Process.*, vol. 10, no. 3, pp. 501-513, Apr. 2016.
- [24] J.-C. Chen, "Hybrid beamforming with discrete phase shifters for millimeter-wave massive MIMO systems," *IEEE Trans. Veh. Technol.*, vol. 66, no. 8, pp. 7604-7608, Aug. 2017.
- [25] Z. Wang, M. Li, Q. Liu, and A. L. Swindlehurst, "Hybrid precoder and combiner design with low-resolution phase shifters in mmWave MIMO systems," *IEEE J. Sel. Topics Signal Process.*, vol. 12, no. 2, pp. 256-269, May 2018.
- [26] J. Zhang, Y. Huang, J. Wang, and L. Yang, "Hybrid Precoding for Wideband Millimeter-Wave Systems With Finite Resolution Phase Shifters," *IEEE Trans. Veh. Technol.*, vol. 67, no. 11, pp. 11285-11290, Nov. 2018.
- [27] X. Gao, L. Dai, Y. Sun, S. Han, and C.-L. I, "Machine learning inspired energy-efficient hybrid precoding for mmWave massive MIMO systems," in *Proc. IEEE Int. Conf. Commun. (ICC)*, Paris, France, May 2017, pp. 1-6.
- [28] Z. Wang, M. Li, H. Li, and Q. Liu, "Hybrid beamforming with one-bit quantized phase shifters in mmWave MIMO systems," in *Proc. IEEE Int. Conf. Commun. (ICC)*, Kansas City, MO, May 2018, pp. 1-6.

- [29] S. Park, A. Alkhateeb, and R. W. Heath, "Dynamic subarrays for hybrid precoding wideband mmWave MIMO systems," *IEEE Trans. Wireless Commun.*, vol. 16, no. 5, pp. 2907-2920, May 2017.
- [30] J. Jin, C. Xiao, W. Chen, and Y. Wu, "Hybrid precoding in mmWave MIMO broadcast channels with dynamic subarrays and finite-alphabet inputs," in *Proc. IEEE Int. Conf. Commun. (ICC)*, Kansas City, MO, May 2018, pp. 1-6.
- [31] Y. Sun, Z. Gao, H. Wang, and D. Wu, "Machine learning based hybrid precoding for mmWave MIMO-OFDM with dynamic subarray," in *Proc. IEEE Global Commun. Conf. (GLOBECOM)*, Abu Dhabi, UAE, Dec. 2018.
- [32] Y. Huang, J. Zhang, and M. Xiao, "Constant envelope hybrid precoding for directional millimeter-wave communications," *IEEE J. Sel. Areas Commun.*, vol. 36, no. 4, Apr. 2018.
- [33] X. Yu, J. Zhang, and K. B. Letaief, "Partially-connected hybrid precoding in mmWave systems with dynamic phase shifter networks," in *Proc. IEEE Int. Workshop on Signal Process. Advances in Wireless Commun. (SPAWC)*, Sapporo, Japan, July 2017, pp. 1-5.
- [34] H. Li, Z. Wang, M. Li, and W. Kellerer, "Efficient analog beamforming with dynamic subarrays for mmWave MU-MISO systems," in *Proc. IEEE Veh. Technol. Conf. (VTC)*, Kuala Lumpur, Malaysia, Apr. 2019.
- [35] H. Li, Z. Wang, Q. Liu, M. Li, "Transmit antenna selection and analog beamforming with low-resolution phase shifters in mmWave MISO systems," *IEEE Commun. Letts.*, vol. 22, no. 9, pp. 1878-1881, Sept. 2018.
- [36] H. Li, Q. Liu, Z. Wang, M. Li, "Joint antenna selection and analog precoder design with low-resolution phase shifters," *IEEE Trans. Veh. Technol.*, vol. 68, no. 1, pp. 967-971, Jan. 2019.
- [37] A. Alkhateeb, Y.-H. Nam, J. Zhang, and R. W. Heath, Jr., "Massive MIMO combining with switches," *IEEE Wireless Commun. Lett.*, vol. 5, no. 3, pp. 232-235, Jun. 2016.
- [38] S. Buzzi, C.-L. I, T. E. Klein, H. V. Poor, C. Yang, and A. Zappone, "A survey of energy-efficient techniques for 5G networks and challenges ahead," *IEEE J. Sel. Areas Commun.*, vol. 34, no. 4, pp. 697-709, Apr. 2016.
- [39] R. Méndez-Rial, C. Rusu, N. González-Prelcic, and A. Alkhateeb, "Hybrid MIMO architectures for millimeter wave communications: Phase shifters or switches?" *IEEE Access*, vol. 4, pp. 247-267, Jan. 2016.
- [40] T. S. Rappaport, G. R. MacCartney, M. K. Samimi, and S. Sun, "Wideband millimeter-wave propagation measurements and channel models for future wireless communication system design," *IEEE Trans. Commun.*, vol. 63, no. 9, pp. 3029-3056, Sept. 2015.
- [41] K. Shen and W. Yu, "Fractional programming for communication systems—Part I: Power control and beamforming," *IEEE Trans. Signal Process.*, vol. 66, no. 10, pp. 2616-2630, May 2018.
- [42] K. Shen and W. Yu, "Fractional programming for communication systems—Part II: Uplink scheduling via matching," *IEEE Trans. Signal Process.*, vol. 66, no. 10, pp. 2631-2644, May 2018.
- [43] P. M. Narendra and K. Fukunaga, "A branch and bound algorithm for feature subset selection," *IEEE Trans. Comput.*, vol. c-26, no. 9, pp. 917-922, Sept. 1977.
- [44] M. Codreanu, A. Tolli, M. Juntti, and M. Latva-aho, "Joint design of TxRx beamformers in MIMO downlink channel," *IEEE Trans. Signal Process.*, vol. 55, no. 9, pp. 4639-4655, Sept. 2007.
- [45] Q. Liu and C. Chen, "Joint transceiver beamforming design and power allocation for multiuser MIMO systems," in *Proc. IEEE Int. Conf. Commun. (ICC)*, Ottawa, Canada, June 2012, pp. 1-5.
- [46] A. Ben-Tal and A. Nemirovski, *Lectures on Modern Convex Optimization: Analysis, Algorithms, and Engineering Applications*. Philadelphia, PA, USA: Society for Industrial and Applied Mathematics, 2001.